

General Paper

Observations of Corrosion Fatigue Crack Initiation Processes in Metals by Means of AFM

Yoshikazu NAKAI, Sanji FUJIWARA, Tomohiro OGAWA, and Yasuki SHIMIZU

*Department of Mechanical Engineering, Kobe University
1-1, Rokkodai, Nada, Kobe 657-8501, Japan*

Abstract: In the present study, corrosion fatigue crack initiation of a 13Cr stainless steel and a high-strength aluminum alloy was investigated by using an atomic force microscopy (AFM). The corrosion fatigue tests of 13Cr stainless steel were conducted in distilled water and dilute sodium chloride solution, and it is found that the corrosion fatigue life was affected by environmental condition. Corrosion fatigue life was found to be shorter for higher concentration of sodium chloride. But no influence of dissolved oxygen was found on corrosion fatigue life. From the surface observation by AFM, no corrosion pits were observed in 100ppm sodium chloride solution before crack initiation. They formed after crack initiation. In 500ppm solution, corrosion fatigue cracks were found to be initiated from surface inclusions. In this solution, corrosion pits were also found at the crack initiation site. The sizes of the pits just after initiation were almost independent of the concentration of sodium chloride. The growth rates of the pits, however, were higher for higher concentration of the solution.

The fatigue strength of 7075-T651 alloy in 3% NaCl solution was also much lower than that in air. Before crack initiation, corrosion pits were observed and corrosion fatigue crack of the alloy was found to be initiated either along the wall of corrosion pit or grain boundary.

Key words: *Corrosion fatigue, Corrosion pit, AFM, Stainless steel, High strength aluminum alloy*

1. INTRODUCTION

Since microscopic observation is the most useful method to clarify the mechanisms of fatigue processes in materials, the progress of metal fatigue study has strongly depended on the development of new microscopic observation methods such as optical microscopy (OM), transmission electron microscopy (TEM), and scanning electron microscopy (SEM). Recently, we obtained a new microscope called as "Scanning Probe Microscope (SPM)", which gives us three-dimensional images of solid surfaces on the atomic scale. It has excellent capabilities for analyzing the topographic nature of solid surfaces. Recently, many types of the scanning probe have been developed. Among SPMs, scanning tunneling microscope (STM) and scanning atomic force microscope (AFM) is now widely employed for the studies of strength of materials because the surface morphology of materials can be observed with atomic scale resolution with these microscopes. By using STM and AFM, Komai and others [1] observed the micro-crack initiation and growth behavior in stress corrosion cracking. Matsuoka and others observed cleavage fracture surface [2]. For fatigue micro-mechanisms, Ishii and others [3] observed fatigue slip band by STM. They also examined fatigue striation shape by AFM [4]. Yoon and others observed nucleation mechanism of intergranular cracks in high-cycle fatigue [5]. Ohgi and others observed crack initiation at grain boundary in low-cycle fatigue [6]. Nakai and his co-workers have been studied on fatigue slip bands, fatigue crack initiation, and the growth behavior of micro-cracks in a structural steel [7] and

α -brass [8-12]. Nakai and Oida [13], Saxena and others [14], and Ogawa and Hatanaka [15] observed the change of surface roughness during fatigue test in air. Nakai and Shimizu studied corrosion pit and crack initiation mechanisms in corrosion fatigue of a stainless steel [16].

In the present paper, corrosion fatigue tests of 13Cr stainless steel and high strength aluminum alloy were conducted in sodium chloride solutions, and crack initiation mechanisms were observed by means of optical microscopy and scanning atomic force microscopy (AFM) to clarify corrosion fatigue crack initiation mechanism.

2. EXPERIMENTAL PROCEDURES

The material for the present study was a 13Cr stainless steel, AISI 414, and a high strength aluminum alloy, 7075-T651. The chemical composition, mechanical properties, and heat treatment conditions of the materials are shown elsewhere [16, 17]. Prior to the fatigue tests, the surface of specimens was polished by buffing.

The specimen has a minimum cross section of width 8 mm and thickness 4 mm, and has weak stress concentration with the elastic stress concentration factor 1.03 under plane bending and 1.13 under push-pull loading.

The fatigue tests were carried out in a computer controlled electro-hydraulic fatigue testing machine or electro-dynamic vibrator operated at a frequency of 30 Hz under fully reversed cyclic loading ($R = -1$). Since it was very difficult to identify in advance where fatigue cracks will be nucleated, we took replicas at the

predetermined number of fatigue cycles. The replica films were coated by Au before observations. Although the height of the surface is reversed from the original surface by the replication method, the height of the replica film in the AFM images was reversed by an image processing technique.

The scanning probe microscope (Seiko Instruments Inc.: SPA-350), which has large stage unit, was employed for the present AFM observation. The resolution of the microscope is 0.5 nm in the surface direction and 0.1 nm in the vertical direction. The region for AFM observation was determined by optical microscopy at a magnification of 2000 on a CRT

monitor.

In the present study, corrosion fatigue tests of the stainless steel were conducted in sodium chloride aqueous solution from 0 to 500 ppm, and the effect of sodium chloride concentration and dissolved oxygen on the corrosion fatigue life and crack initiation mechanism were examined. The corrosion fatigue tests of the aluminum alloy were conducted in 3% sodium chloride aqueous solution.

3. EXPERIMENTAL RESULTS AND DISCUSSION

3.1. 13Cr Stainless Steel

3.1.1. S-N curve

Figure 1 shows the relation between stress amplitude, σ_a , and number of cycles to failure, N_f , under push-pull loading. The fatigue life in aqueous environments is shorter than that in air. Among the aqueous environments, the fatigue life in 10 ppm NaCl solution is almost the same for that in distilled water. The fatigue life in 100 ppm NaCl solution, however, is shorter than that either in 10 ppm solution or in distilled water. For either concentration of NaCl solution, the fatigue life in aerated solution is almost the same for that in deaerated solution.

In push-pull loading, some cracks were initiated from the cylindrically curved side surface. Since it was easier to observe in plane surface than in curved surface when the magnification of the microscope was high, plane bending fatigue tests were conducted. There were no significant difference in fatigue life between plane bending and push-pull loading [16].

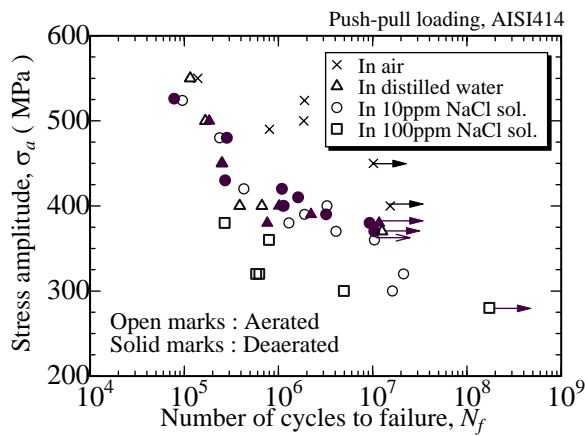


Fig. 1. S-N curves.

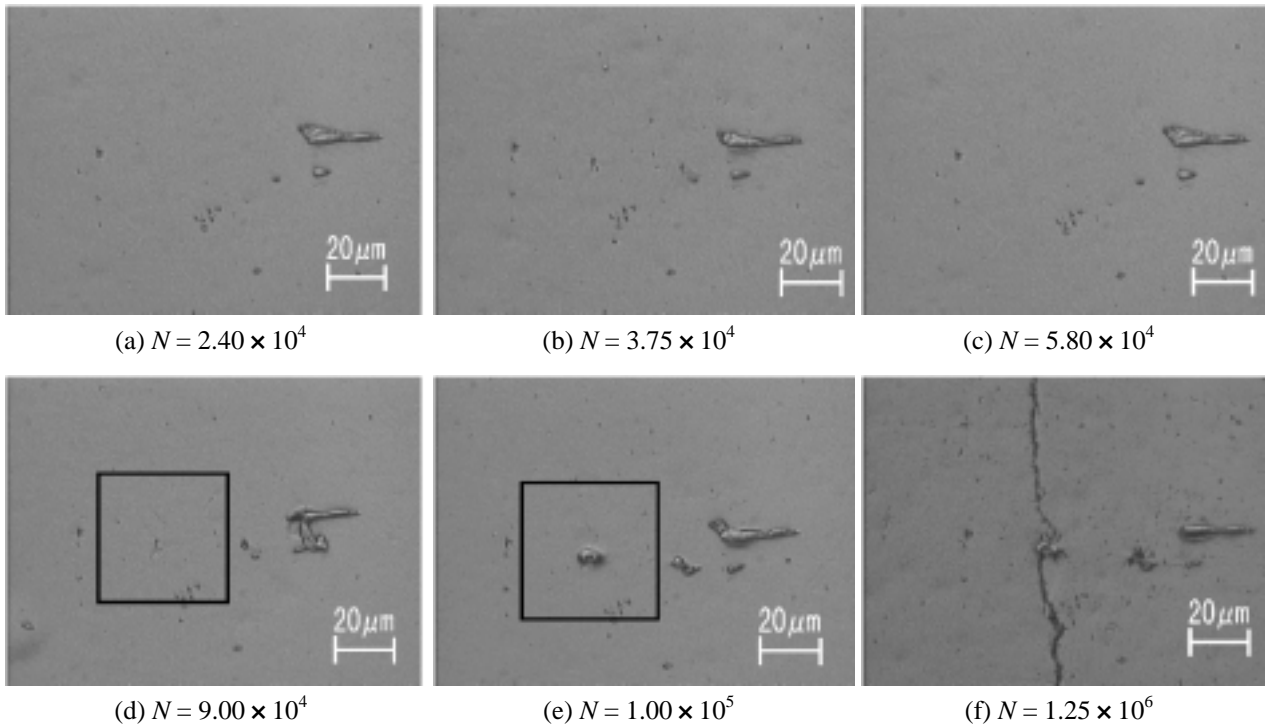


Fig. 2. Optical micrographs of fatigued specimen surfaces in 100 ppm NaCl solution at $\sigma_a = 430$ MPa.

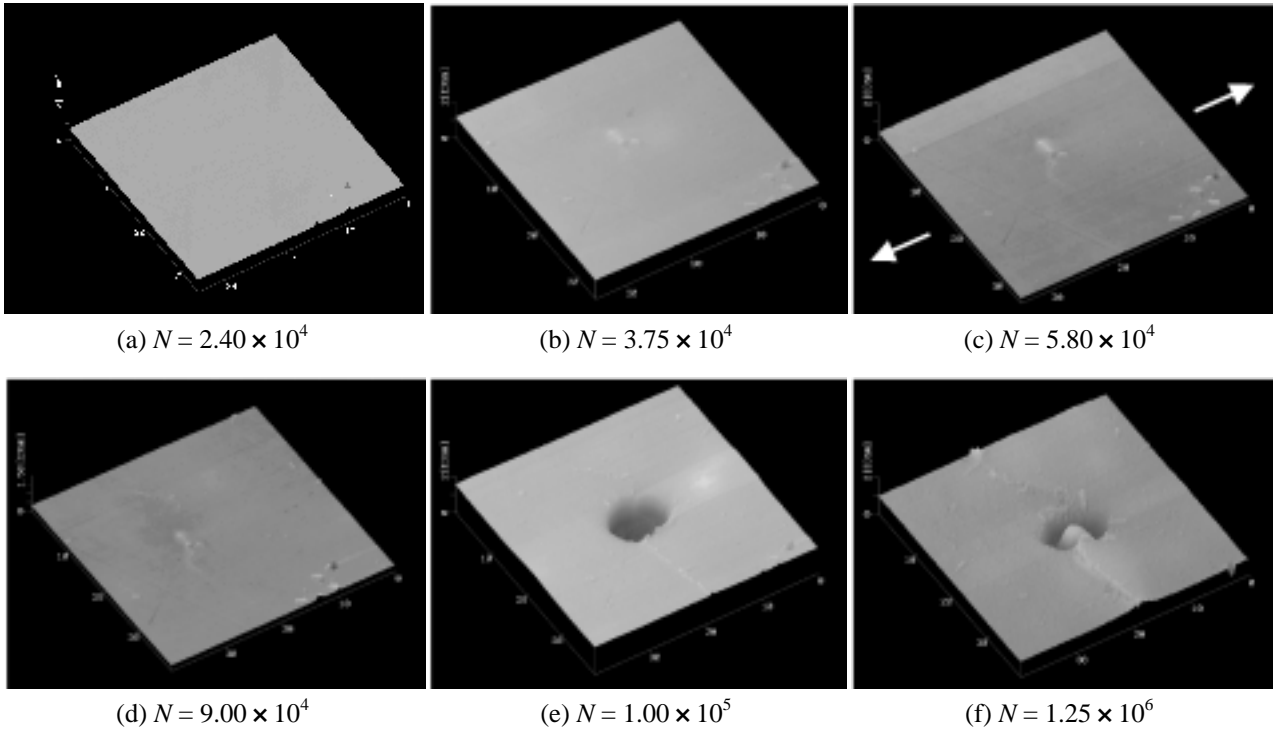


Fig. 3. AFM images of surfaces in 100 ppm NaCl solution at $\sigma_a = 430$ MPa (Scanning area: $35 \mu\text{m} \times 35 \mu\text{m}$).

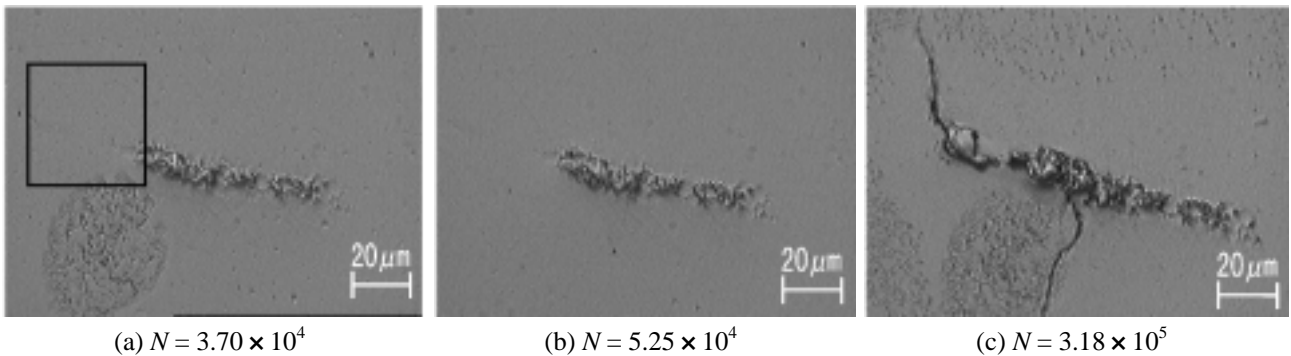


Fig. 4. Optical micrographs of surfaces in 500 ppm NaCl solution at $\sigma_a = 430$ MPa.

3.1.2. Crack initiation process

Either in distilled water and in 10 ppm sodium chloride solution, no cracks were initiated from corrosion pits, then the mechanism of crack initiation in these solutions may almost the same for that in air.

Optical micrographs of specimen surface fatigued in aerated 100 ppm NaCl aqueous solution at $\sigma_a = 430$ MPa are shown in Fig. 2. In these micrographs, it seems that a corrosion pit was formed at $N = 1.00 \times 10^5$ cycles and a crack was initiated from the corrosion pit.

AFM images of the same area are shown in Fig. 3. In these images, extrusions are found in (b)($N=3.75 \times 10^4$), and a crack was initiated from the extrusions in (c)($N=5.80 \times 10^4$). The extrusion is considered to be corrosion product, which was formed at bare metal surface produced by a crack embryo. A corrosion pit

was formed at the crack initiation site in (e)($N=1.00 \times 10^5$). Then, it is obvious from the AFM observation that the fatigue crack was initiated before the corrosion pit appeared. A corrosion pit was found to be initiated along the crack. Therefore, it is important to notice that we sometimes misunderstand about corrosion fatigue crack initiation process from optical microscopy. To combine AFM observations with optical microscopy, we can well understand corrosion fatigue process.

Optical micrographs of specimen surface fatigued in aerated 500 ppm NaCl aqueous solution at $\sigma_a = 430$ MPa are shown in Fig. 4. In 500 ppm sodium chloride solution, fatigue cracks were found to be initiated from surface inclusions. At $N = 5.25 \times 10^4$ cycles, a crack was formed at left end of an inclusion. Figures 5 and 6 are AFM images of the same region shown in Fig. 5, where images in Fig. 6 is higher magnification images of

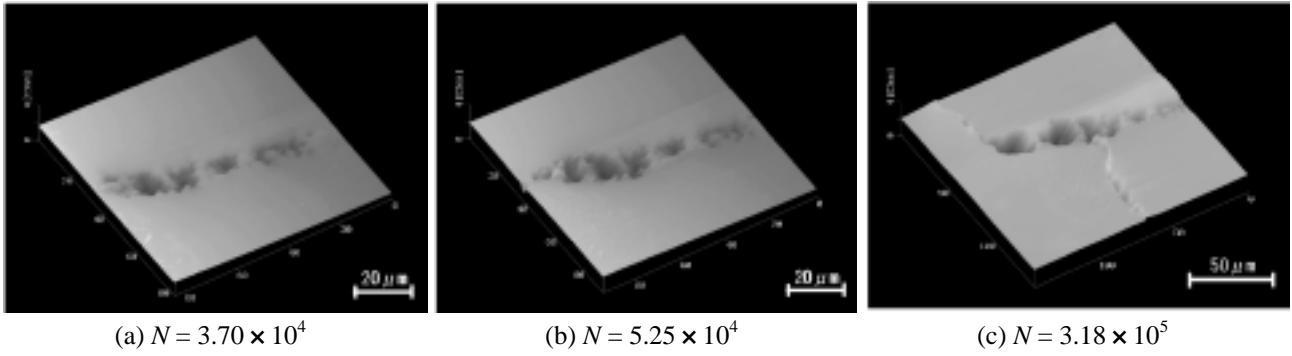


Fig. 5. AFM images of surfaces in 500 ppm NaCl solution at $\sigma_a = 430$ MPa.

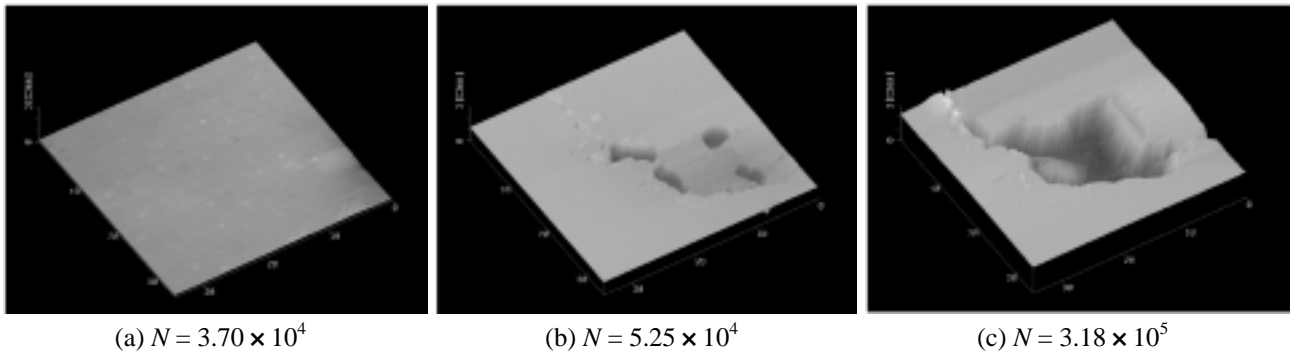


Fig. 6. AFM images of surfaces in 500 ppm NaCl solution at $\sigma_a = 430$ MPa ($35 \mu\text{m} \times 35 \mu\text{m}$).

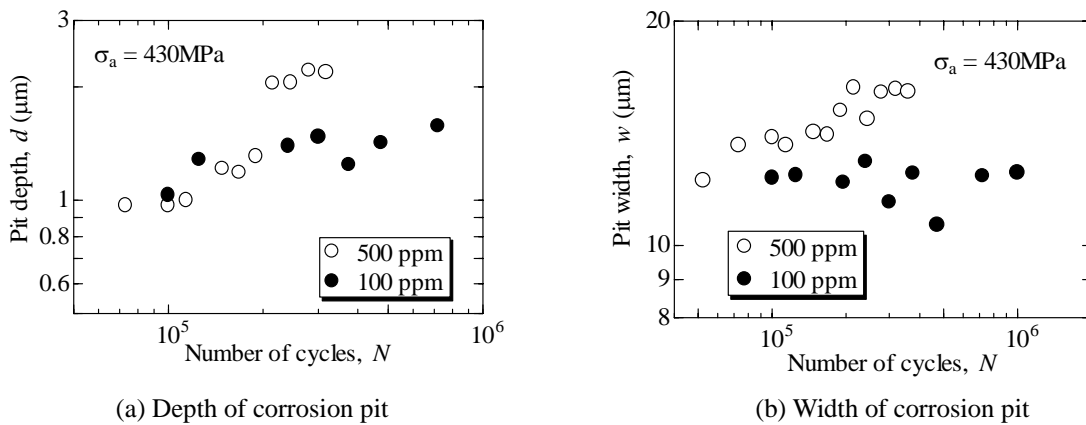


Fig. 7. Growth of pits in corrosion fatigue.

the crack initiation site of the inclusion. In this case, corrosion pits were appeared almost at the same time of the crack initiation.

Inclusions also existed in specimens those were fatigued in 10 ppm solution, 100 NaCl solution, and in distilled water, but they were not crack initiation site in these environments

3.1.3. Growth behavior of corrosion pits

Depth and surface width of a corrosion pit can be measured from cross-section geometry of the pits, which can be obtained from AFM image.

Changes in the size of corrosion pits are plotted as a

function of number of cycles in Fig. 7, where pit width was measured perpendicular to the loading direction, The stress amplitude for these observation was 430 MPa, and the concentration of NaCl was either 100 ppm or 500 ppm. Although the sizes of corrosion pits just after initiation was almost independent of the concentration of NaCl, the growth rate of the pits was higher for higher concentration of NaCl.

Change of aspect ratio of corrosion pits in fatigue is shown in Fig. 8. The aspect ratio was almost independent of the concentration of NaCl, and it gradually increased with number of cycles. The aspect

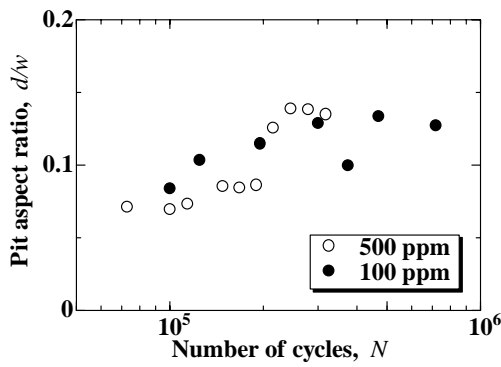


Fig. 8. Change of aspect ratio of corrosion pits in fatigue.

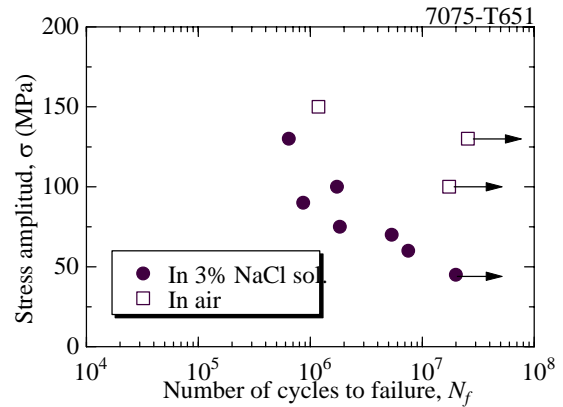


Fig. 9. S-N curves (Plane bending).

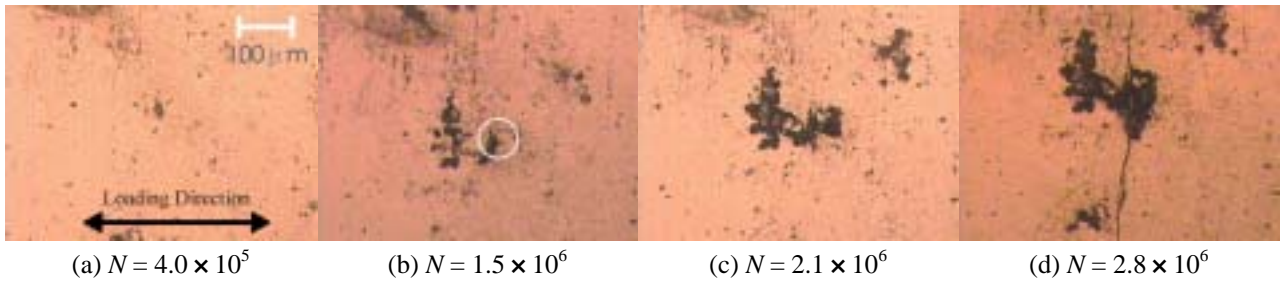


Fig. 10. Optical microscopy.

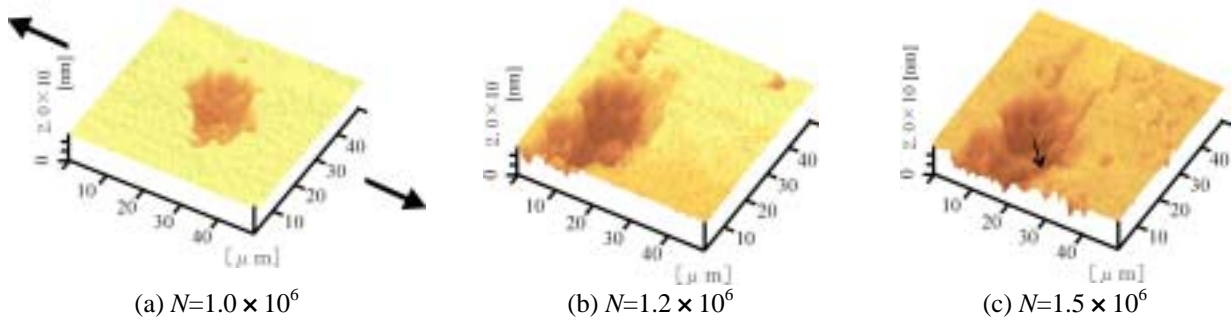


Fig. 11. Scanning atomic force microscopy.

ratio, however, remained 0.14 at the final stage of corrosion fatigue, then, the stress concentration by these pits were small.

3.2. High Strength Aluminum Alloy

3.2.1. S-N curve

Figure 9 shows the relation between stress amplitude, σ_a , and number of cycles to failure, N_f . In 3% NaCl aqueous solution, fatigue limit was not observed for this material, and the fatigue life in aqueous environments is much shorter than that in air.

3.2.2. Crack initiation from corrosion pit

Optical microscopies of the specimen surface fatigue at a stress amplitude of 100 MPa were shown in Fig. 10. The corrosion pit was initiated at very early stage of fatigue test, and it grew with number of cycles, and a crack was initiated from the pit.

The crack initiation at $N = 1.5 \times 10^6$ could be

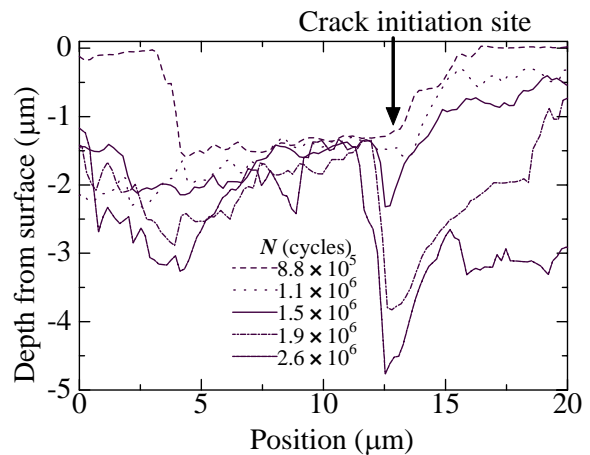


Fig. 12. Changes of cross section geometry.

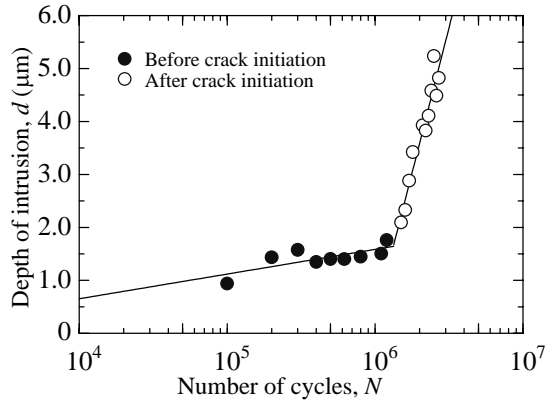


Fig. 13. Change of intrusion depth in fatigue process.

identified more clearly from AFM images, those are shown in Fig. 11. In these figures, arrows indicate the loading direction. Change of the geometry of cross-section is indicated in Fig. 12. No cracks were initiated from the deepest point of the corrosion pit. It was initiated at a grain-boundary within the pit. As shown in Fig. 13, the growth rate of intrusion depth at crack initiation site was accelerated with crack initiation.

3.2.3. Crack initiation from grain-boundary

Another example of AFM images of crack initiation is shown in Fig. 14. No corrosion pit was observed from the optical micrograph (see Fig. 14 (a)), while the AFM image shown in Fig. 14 (b) indicates that there was a small pit at the crack initiation site, and it propagated along the grain boundary (see Fig. 14 (c)). In this case it was not clear whether the pit was nucleated after or before crack initiation.

4. CONCLUSIONS

Corrosion fatigue tests of a 13Cr stainless steel and a high strength aluminum alloy were conducted in sodium chloride solutions, and the initiation process of cracks and corrosion pits were observed by means of optical microscopy and scanning atomic-force microscopy. The following results were obtained.

(1) In both materials, the fatigue life in aqueous environment was shorter than that in air. In the stainless steel, the corrosion fatigue life was shorter for higher concentration of sodium chloride. But no

influence of dissolved oxygen was found on corrosion fatigue life.

(2) In the stainless steel, no cracks were initiated at corrosion pits when the concentration of sodium chloride was less than 10 ppm. In 500ppm solution, cracks were found to be initiated from surface inclusions. In this solution, corrosion pits were also found at the crack initiation site.

(3) In the aluminum alloy, cracks were initiated either at corrosion pit or grain boundary. For crack initiation at corrosion pit, it was not nucleated from the deepest point of the pit. The crack initiation site within the pit was also the grain boundary.

REFERENCES

1. K. Komai, K. Minoshima, and M. Itoh, J. Soc. Mat. Sci., Japan, **43** (1994), 336 (in Japanese).
2. S. Matsuoka, H. Sumiyoshi, K. Ishikawa, Trans. Japan Soc. Mech. Eng., **56A** (1990), 2091 (in Japanese).
3. H. Ishii, S. Yamanaka, and K. Tohgo, Proc. 7th Int. Conf. Mech. Behav. Mat. (ICM 7) (1995), 367.
4. S. Choi, H. Ishii, and K. Tohgo, J. Mat. Sci., Japan, **47**, (1998), 852-857 (in Japanese).
5. W. K. Yoon, T. Inoue, H. Noguchi, and K. Higashida, Trans. JSME, **64A** (1998), 1435 (in Japanese).
6. J. Ohgi, K. Hatanaka, T. Zenge, Proc. 11th Int. Conf. Experimental Mechanics (1998), 1053.
7. Y. Nakai, S. Fukuhara, and K. Ohnishi, Int. J. Fatigue, **19S**, (1997), 223.
8. Y. Nakai, K. Ohnishi, and T. Kusukawa, Trans. Jpn Soc. Mech. Eng., **65A** (1999), 483 (in Japanese).
9. Y. Nakai, K. Ohnishi, and T. Kusukawa, Small Fatigue Cracks: Mechanics and Mechanisms, (ed. by K. S. Ravichandran, R. O. Ritchie, and Y. Murakami) (1999), 343.
10. Y. Nakai, T. Kusukawa, and N. Hayashi, Proc. ATEM'99, Vol. 1 (1999), 152.
11. Y. Nakai and T. Kusukawa, To be published in Trans. Jpn Soc. Mech. Eng., **67A** (2001) (in Japanese).
12. Y. Nakai and T. Kusukawa, N. Hayashi, ASTM STP (submitted).
13. Y. Nakai and M. Oida, Fatigue '99 (1999), 2771.
14. A. Saxena, F. Yang, and L. Cretegnny, Fatigue '99, (1999), 2777.
15. H. Ogawa and K. Hatanaka, Proc. ATEM'99, Vol. 1 (1999), 158.
16. Y. Nakai, Y. Shimizu, and N. Saeki, Progress in Mechanical Behavior of Materials (ICM8) (ed. by F. Ellyin and J. W. Provan), Vol. I (1999), 364.
17. Y. Nakai, K. Kondo, and K. Ohji, Trans. Jpn Soc. Mech. Eng., **58A** (1992), 359 (in Japanese).

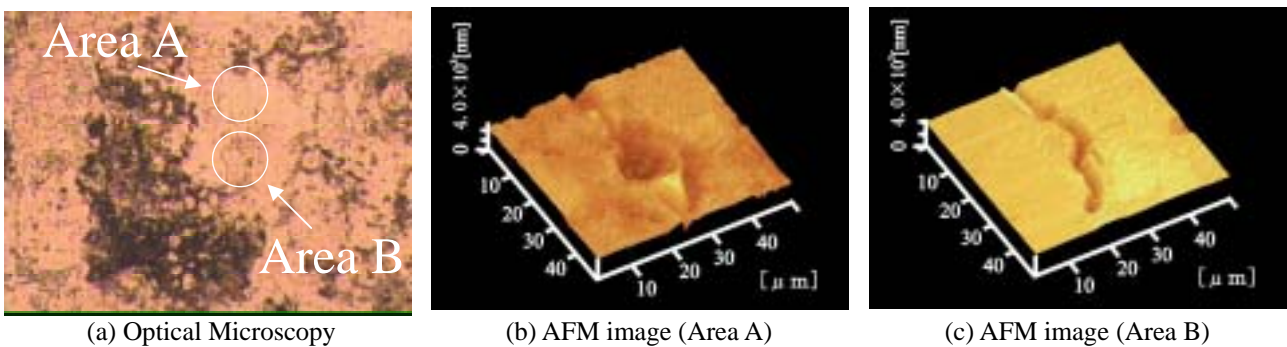


Fig. 14. Crack initiation from grain boundary ($\sigma_a = 80$ MPa, 7.94×10^5).